WELL-BALANCED CENTRAL SCHEME FOR THE SYSTEM OF MHD EQUATIONS WITH GRAVITATIONAL SOURCE TERM

FARAH KANBAR*, RONY TOUMA †, AND CHRISTIAN KLINGENBERG*

Abstract. A well-balanced second order finite volume central scheme for the magnetohydrodynamic (MHD) equations with gravitational source term is developed in this paper. The scheme is an unstaggered central scheme that evolves the numerical solution on a single grid and avoids solving Riemann problems at the cell interfaces using ghost staggered cells. A subtraction technique is used on the conservative variables with the support of a known steady state in order to manifest the well-balanced property of the scheme. The divergence-free constraint of the magnetic field is satisfied after applying the constrained transport method (CTM) for unstaggered central schemes at the end of each time-step by correcting the components of the magnetic field. The robustness of the proposed scheme is verified on a list of numerical test cases from the literature.

Key words. MHD equations, unstaggered central schemes, well-balanced schemes, steady states, divergence-free constraint, constrained transport method.

AMS subject classifications. 65M08, 76M12, 65M22.

1. Introduction. Ideal Magnetohydrodynamics (MHD) equations model problems in physics and astrophysics. The MHD system is a combination of the Navier-Stokes equations of fluid dynamics and the Maxwell equations of electromagnetism. A gravitational source term is added to the ideal MHD equations in two space dimensions in order to model more complicated problems arising in astrophysics and solar physics such as modeling wave propagation in idealized stellar atmospheres [16, 3]. From electromagnetic theory, the magnetic field $\mathbf{B}$ must be solenoidal i.e. $\nabla \cdot \mathbf{B} = 0$ at all times. The divergence-free constraint on the magnetic field reflects the fact that magnetic mono-poles have not been observed in nature. The induction equation for updating the magnetic field imposes the divergence on the magnetic field. Hence, a numerical scheme for the MHD equations should maintain the divergence-free property of the discrete magnetic field at each time-step. Numerical schemes usually fail to satisfy the divergence-free constraint and numerical instabilities and unphysical oscillations may be observed [17]. Several methods were developed to overcome this issue. The projection method, in which the magnetic field is projected into a zero divergence field by solving an elliptic equation at each time step [4].

Another procedure is the Godunov-Powell procedure [14, 12, 7], where the Godunov-Powell form of the system of the MHD equations is discretized instead of the original system. The Godunov-Powell system has the divergence of the magnetic field as a part of the source term. Hence, divergence errors are transported out of the domain with the flow.

A third approach is the CTM [5, 15, 6]. The CTM was modified from its original form to the case of staggered central schemes [1]. It was later extended to the case of unstaggered central schemes [19]. Hence, a numerical scheme for the MHD equations should maintain the divergence-free property of the discrete magnetic field at each time-step. A finite volume second-order accurate unstaggered central scheme is used to model the MHD equations with a gravitational source term. Finite volume central schemes were first introduced in 1990 by Nessyahu and Tadmor (NT) [11]. The NT scheme is based on evolving piecewise linear numerical solution on two staggered grids.

*University of Wuerzburg, Wuerzburg, Germany.
†Lebanese American University, Beirut, Lebanon.

The most significant property of central schemes is that they avoid solving Riemann problems arising at the cell interfaces. Our scheme is UC (unstaggered central) type scheme that was first developed in [9, 18]. These schemes allow the evolution of the numerical solution on a single grid instead of using two different grids. UC schemes were first developed for hyperbolic systems of conservation laws and then extended to hyperbolic systems of balance laws[23, 21, 22, 20]. The UC schemes introduced the possibility of avoiding solving Riemann problems and switching between two grids. The approach is achieved by the help of ghost staggered cells used implicitly to avoid Riemann problems at the cell interfaces.
In the presence of a gravitational source term on the right hand side of the MHD system, one has to consider a well-balanced technique that provides the numerical scheme with the ability to preserve hydrostatic equilibrium. In this paper we extend the reconstruction technique on the conservative variables, previously developed in [2, 10] for the system of Euler equations, for the system of MHD equations. The idea is to evolve the error function between the vector of conserved variables and a given steady state, instead of evolving the vector of conserved variables. This error function is defined as $\mathbf{\Delta U} = \mathbf{U} - \tilde{\mathbf{U}}$, where $\tilde{\mathbf{U}}$ is a given steady state. Knowing the steady state (analytically or numerically) is a key ingredient for the implementation of the proposed scheme.
The paper is divided into the following sections. The MHD model is presented in section 2 and the finite volume scheme is described in section 3 followed by the CTM in section 4. Numerical experiments are illustrated in section 5 and finally some concluding remarks and future work are given in section 6.

2. The model.

2. The model. The system of MHD equations with gravitational source term in two space dimensions is given by:

$$\begin{cases} \mathbf{U}_t + F(\mathbf{U})_x + G(\mathbf{U})_y = S(\mathbf{U}), & (x,y) \in \Omega \subset \mathbb{R}^2,\ t > 0. \\ \mathbf{U}(x,y,0) = \mathbf{U}_0(x,y), \end{cases} \tag{2.1}$$

where

$$\mathbf{U} = \begin{pmatrix} \rho \\ \rho u_1 \\ \rho u_2 \\ \rho u_3 \\ E \\ B_1 \\ B_2 \\ B_3 \end{pmatrix},\ F(\mathbf{U}) = \begin{pmatrix} \rho u_1 \\ \rho u_1^2 + \Pi_{11} \\ \rho u_1 u_2 + \Pi_{12} \\ \rho u_1 u_3 + \Pi_{13} \\ E u_1 + u_1 \Pi_{11} + u_2 \Pi_{12} + u_3 \Pi_{13} \\ 0 \\ \Lambda_2 \\ -\Lambda_3 \end{pmatrix},$$

$$G(\mathbf{U}) = \begin{pmatrix} \rho u_2 \\ \rho u_2 u_1 + \Pi_{21} \\ \rho u_2^2 + \Pi_{22} \\ \rho u_2 u_3 + \Pi_{23} \\ E u_2 + u_1 \Pi_{21} + u_2 \Pi_{22} + u_3 \Pi_{23} \\ -\Lambda_3 \\ 0 \\ \Lambda_1 \end{pmatrix}, S(\mathbf{U}) = \begin{pmatrix} 0 \\ 0 \\ -\rho \phi_y \\ 0 \\ -\rho u_2 \phi_y \\ 0 \\ 0 \\ 0 \end{pmatrix}.$$

Here ρ is the fluid density, $\rho\mathbf{u}$ is the momentum with $\mathbf{u} = (u_1, u_2, u_3)$, p is the pressure, $\mathbf{B} = (B_1, B_2, B_3)$ is the magnetic field, and E is the kinetic and internal energy of the fluid given by the following equation $E = \frac{p}{\gamma-1} + \frac{1}{2}\rho|\mathbf{u}|^2 + \frac{1}{2}|\mathbf{B}|^2$ with γ the ratio

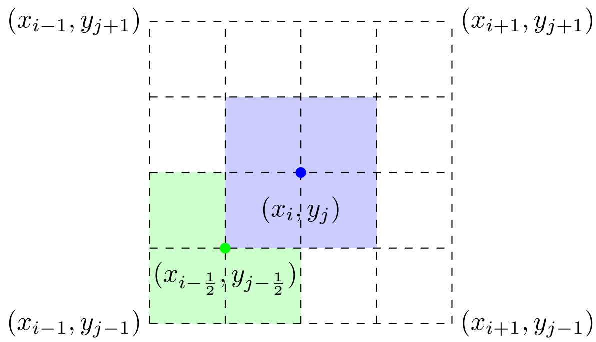

Fig. 1: The cells of the main grid $C_{i,j}$ (blue cell) and of the staggered grid $D_{i-\frac{1}{2},j-\frac{1}{2}}$ (green cell).

of specific heats. $\phi = \phi(x, y)$, with $\phi_x = 0$ and $\phi_y = g$, is the gravitational potential and it is a given function. The conservation of the total energy (internal, kinetic and magnetic) has the gravitational potential energy as a source term. $\Lambda = \mathbf{u} \times \mathbf{B}$, Π_{11}, Π_{22} and Π_{33} are the diagonal elements of the total pressure tensor and Π_{12}, Π_{13} and Π_{23} are the off-diagonal tensor are given by the following formulas:
$\Pi_{ii} = p + \frac{1}{2}(B_j^2 + B_k^2 - B_i^2)$ and $\Pi_{ij} = -\frac{1}{2}B_i B_j$, for $i, j, k = 1, 2, 3$.
To determine the time-step using the CFL condition, we present the eigenvalues of the flux jacobian in the x-direction,
$\lambda_1 = u_1 - c_f$, $\lambda_2 = u_1 - b_1$, $\lambda_3 = u_1 - c_s$, $\lambda_4 = u_1$, $\lambda_5 = u_1$, $\lambda_6 = u_1 + c_s$, $\lambda_7 = u_1 + b_1$, $\lambda_8 = u_1 + c_f$. The eigenvalues of the flux jacobian in the y-direction are analogously defined.
Here,

$$c_f = \sqrt{\frac{1}{2}\left(a^2 + b^2 + \sqrt{\left(a^2 + b^2\right)^2 - 4a^2 b_1^2}\right)}, \tag{2.2}$$

and

$$c_s = \sqrt{\frac{1}{2}\left(a^2 + b^2 - \sqrt{\left(a^2 + b^2\right)^2 - 4a^2 b_1^2}\right)}, \tag{2.3}$$

are respectively the fast and slow wave speeds with $a = \sqrt{\frac{\gamma p}{\rho}}$ is the sound speed and $b = \sqrt{b_1^2 + b_2^2 + b_3^2}$ with $b_i = \frac{B_i}{\sqrt{\rho}}, i \in \{1, 2, 3\}$. For additional reading on the hyperbolic analysis of the system, readers are refered to [8, 13].

3. The unstaggered two-dimensional finite volume central scheme. We consider a Cartesian decomposition of the computational domain Ω where the control cells are the rectangles $C_{i,j} = \left[x_{i-\frac{1}{2}}, x_{i+\frac{1}{2}}\right] \times \left[y_{j-\frac{1}{2}}, y_{j+\frac{1}{2}}\right]$ centered at the nodes (x_i, y_j). We define the dual staggered cells $D_{i+\frac{1}{2},j+\frac{1}{2}} = [x_i, x_{i+1}] \times [y_j, y_{j+1}]$ centered at $(x_{i+\frac{1}{2}}, y_{j+\frac{1}{2}})$. Here, $x_{i+\frac{1}{2}} = x_i + \frac{\Delta x}{2}$ and $y_{j+\frac{1}{2}} = y_j + \frac{\Delta y}{2}$, where $\Delta x = x_{i+\frac{1}{2}} - x_{i-\frac{1}{2}}$ and $\Delta y = y_{j+\frac{1}{2}} - y_{j-\frac{1}{2}}$. The visualization of the 2D grids is given in figure 1. Before proceeding with the derivation of the 2D numerical method, and for convenience, we introduce the average value notations:

$$\overline{\rho}_{i,j+\frac{1}{2}} = \frac{\rho_{i,j}+\rho_{i,j+1}}{2}, \overline{\rho}_{i+\frac{1}{2},j} = \frac{\rho_{i,j}+\rho_{i+1,j}}{2}, \overline{\rho}_{i,(j)} = \frac{\rho_{i,j+\frac{1}{2}}+\rho_{i,j-\frac{1}{2}}}{2}$$

$$\overline{\rho}_{(i),j} = \frac{\rho_{i+\frac{1}{2},j}+\rho_{i-\frac{1}{2},j}}{2}, \quad [[\rho]]_{i,j+\frac{1}{2}} = \rho_{i,j+1}-\rho_{i,j}$$

$$[[\rho]]_{i+\frac{1}{2},j} = \rho_{i+1,j}-\rho_{i,j},\ [[\rho]]_{i,(j)} = \rho_{i,j+\frac{1}{2}}-\rho_{i,j-\frac{1}{2}},\ [[\rho]]_{(i),j} = \rho_{i+\frac{1}{2},j}-\rho_{i-\frac{1}{2},j}.$$

We assume that $\tilde{\mathbf{U}}$ is a given stationary solution of system (2.1) and we define $\Delta\mathbf{U} = \mathbf{U}-\tilde{\mathbf{U}}$. We substitute $\mathbf{U} = \Delta\mathbf{U}+\tilde{\mathbf{U}}$ in the balance law (2.1), we obtain:

$$(\Delta\mathbf{U})_t + F(\Delta\mathbf{U}+\tilde{\mathbf{U}})_x + G(\Delta\mathbf{U}+\tilde{\mathbf{U}})_y = S(\Delta\mathbf{U}+\tilde{\mathbf{U}},x,y). \tag{3.1}$$

On the other hand, since $\tilde{\mathbf{U}}$ is a stationary solution, then balance law in (2.1) reduces to

$$F(\tilde{\mathbf{U}})_x + G(\tilde{\mathbf{U}})_y = S(\tilde{\mathbf{U}},x,y). \tag{3.2}$$

Subtracting equation (3.2) from equation (3.1), we obtain

$$\begin{aligned}(\Delta\mathbf{U})_t + [F(\Delta\mathbf{U}+\tilde{\mathbf{U}}) - F(\tilde{\mathbf{U}})]_x + [G(\Delta\mathbf{U}+\tilde{\mathbf{U}}) - G(\tilde{\mathbf{U}})]_y \\ = S(\Delta\mathbf{U}+\tilde{\mathbf{U}},x,y) - S(\tilde{\mathbf{U}},x,y).\end{aligned} \tag{3.3}$$

Using the fact that the source term $S(\mathbf{U},x,y)$ in (2.1) is linear in terms of the conserved variables, then equation (3.3) reduces to

$$(\Delta\mathbf{U})_t + [F(\Delta\mathbf{U}+\tilde{\mathbf{U}}) - F(\tilde{\mathbf{U}})]_x + [G(\Delta\mathbf{U}+\tilde{\mathbf{U}}) - G(\tilde{\mathbf{U}})]_y = S(\Delta\mathbf{U},x,y). \tag{3.4}$$

The proposed numerical scheme consists of evolving the balance law (3.4) instead of evolving the balance law in system (2.1).
The numerical solution $\mathbf{U}$ will be then obtained using the formula $\mathbf{U} = \Delta\mathbf{U}+\tilde{\mathbf{U}}$. The numerical scheme that we shall use to evolve $\Delta\mathbf{U}(x,y,t)$ follows a classical finite volume approach; it evolves a piecewise linear function $\mathcal{L}_{i,j}(x,y,t)$ defined on the control cells $C_{i,j}$ and used to approximate the analytic solution $\Delta\mathbf{U}(x,y,t)$ of system (2.1). Without any loss of generality we can assume that $\Delta\mathbf{U}^n_{i,j}$ is known at time t^n and we define $\mathcal{L}_{i,j}(x,y,t^n)$ on the cells $C_{i,j}$ as follows.

$$\mathcal{L}_{i,j}(x,y,t^n) = \Delta\mathbf{U}^n_{i,j} + (x-x_i)\frac{(\Delta\mathbf{U}^{n,x}_{i,j})'}{\Delta x} + (y-y_j)\frac{(\Delta\mathbf{U}^{n,y}_{i,j})'}{\Delta y}, \qquad \forall (x,y)\in C_{i,j},$$

where $\frac{(\Delta\mathbf{U}^{n,x}_{i,j})'}{\Delta x}$ and $\frac{(\Delta\mathbf{U}^{n,y}_{i,j})'}{\Delta y}$ are limited numerical gradients approximating $\frac{\partial\Delta\mathbf{U}}{\partial x}(x,y_j,t^n)|_{x=x_i}$ and $\frac{\partial\Delta\mathbf{U}}{\partial y}(x_i,y,t^n)|_{y=y_j}$, respectively, at the point (x_i,y_j,t^n). In order to approximate the spatial numerical derivatives, the (MC-θ) limiter is considered which is defined as

$$(\Delta\mathbf{u}^n_i)' = \text{minmod}\left[\theta\left(\Delta\mathbf{u}^n_i - \Delta\mathbf{u}^n_{i-1}\right), \frac{\Delta\mathbf{u}^n_{i+1}-\Delta\mathbf{u}^n_{i-1}}{2}, \theta\left(\Delta\mathbf{u}^n_{i+1}-\Delta\mathbf{u}^n_i\right)\right] \tag{3.5}$$

where θ is a parameter such that $1<\theta<2$, while the minmod function is defined as:

$$\text{minmod}(a,b,c) = \begin{cases}\text{sign}(a)\text{min}\{|a|,|b|,|c|\}, & \text{if sign}(a)=\text{sign}(b)=\text{sign}(c)\\ 0, & \text{Otherwise.}\end{cases}$$

The (MC-θ) limiter (3.5) is used to compute the quantities $(\Delta\mathbf{U}^{n,x}_{i,j})'$ and $(\Delta\mathbf{U}^{n,y}_{i,j})'$ in order to avoid spurious oscillations. Next, we integrate the balance law (3.4) over the rectangular box $R^n_{i+\frac{1}{2},j+\frac{1}{2}} = D_{i+\frac{1}{2},j+\frac{1}{2}} \times [t^n, t^{n+1}]$,

$$\iiint_{R_{i+\frac{1}{2},j+\frac{1}{2}}} (\Delta\mathbf{U})_t + [F(\Delta\mathbf{U}+\tilde{\mathbf{U}}) - F(\tilde{\mathbf{U}})]_x + [G(\Delta\mathbf{U}+\tilde{\mathbf{U}}) - G(\tilde{\mathbf{U}})]_y dR = \iiint_{R_{i+\frac{1}{2},j+\frac{1}{2}}} S(\Delta\mathbf{U}, x, y) dR. \tag{3.6}$$

We use the fact that $\Delta\mathbf{U}$ is approximated using piecewise linear interpolants similar to $\mathcal{L}_{i,j}$ on the cells $C_{i,j}$; following the derivation of the unstaggered central schemes in [18], equation (3.6) is rewritten as:

$$\Delta\mathbf{U}^{n+1}_{i+\frac{1}{2},j+\frac{1}{2}} = \Delta\mathbf{U}^{n}_{i+\frac{1}{2},j+\frac{1}{2}} - \frac{1}{\Delta x \Delta y} \iiint_{R_{i+\frac{1}{2},j+\frac{1}{2}}} [F(\Delta\mathbf{U}+\tilde{\mathbf{U}}) - F(\tilde{\mathbf{U}})]_x + [G(\Delta\mathbf{U}+\tilde{\mathbf{U}}) - G(\tilde{\mathbf{U}})]_y dR + \frac{1}{\Delta x \Delta y} \iiint_{R_{i+\frac{1}{2},j+\frac{1}{2}}} S(\Delta\mathbf{U}, x, y) dR. \tag{3.7}$$

For the flux integrals, we apply the divergence theorem that converts the volume integral into a surface integral. Equation (3.7) becomes then:

$$\begin{aligned}\Delta\mathbf{U}^{n+1}_{i+\frac{1}{2},j+\frac{1}{2}} = \Delta\mathbf{U}^{n}_{i+\frac{1}{2},j+\frac{1}{2}} &- \frac{1}{\Delta x \Delta y} \int_{t^n}^{t^{n+1}} \int_{\partial R_{xy}} [F(\Delta\mathbf{U}+\tilde{\mathbf{U}}) - F(\tilde{\mathbf{U}})] \cdot n_x dA dt \\ &- \frac{1}{\Delta x \Delta y} \int_{t^n}^{t^{n+1}} \int_{\partial R_{xy}} [G(\Delta\mathbf{U}+\tilde{\mathbf{U}}) - G(\tilde{\mathbf{U}})] \cdot n_y dA dt \\ &+ \frac{1}{\Delta x \Delta y} \iiint_{R_{i+\frac{1}{2},j+\frac{1}{2}}} S(\Delta\mathbf{U}, x, y) dR,\end{aligned} \tag{3.8}$$

where $R_{xy} = [x_i, x_{i+1}] \times [y_i, y_{i+1}]$, and $\mathbf{n} = (n_x, n_y)$ is the outward pointing unit normal at each point on the boundary ∂R_{xy}(the boundary of R_{xy}), see figure 2. The integral of the source term is being approximated using the midpoint quadrature rule both in time and space:

$$\iiint_{R_{i+\frac{1}{2},j+\frac{1}{2}}} S(\Delta\mathbf{U}) dR = \Delta x \Delta y \Delta t S(\Delta\mathbf{U}^{n+\frac{1}{2}}_{i,j}, \Delta\mathbf{U}^{n+\frac{1}{2}}_{i+1,j}, \Delta\mathbf{U}^{n+\frac{1}{2}}_{i,j+1}, \Delta\mathbf{U}^{n+\frac{1}{2}}_{i+1,j+1}), \tag{3.9}$$

with

$$S(\Delta\mathbf{U}^{n+\frac{1}{2}}_{i,j}, \Delta\mathbf{U}^{n+\frac{1}{2}}_{i+1,j}, \Delta\mathbf{U}^{n+\frac{1}{2}}_{i,j+1}, \Delta\mathbf{U}^{n+\frac{1}{2}}_{i+1,j+1}) = \left[\frac{S(\Delta\mathbf{U}^{n+\frac{1}{2}}_{i,j}) + S(\Delta\mathbf{U}^{n+\frac{1}{2}}_{i+1,j}) + S(\Delta\mathbf{U}^{n+\frac{1}{2}}_{i,j+1}) + S(\Delta\mathbf{U}^{n+\frac{1}{2}}_{i+1,j+1})}{4}\right].$$

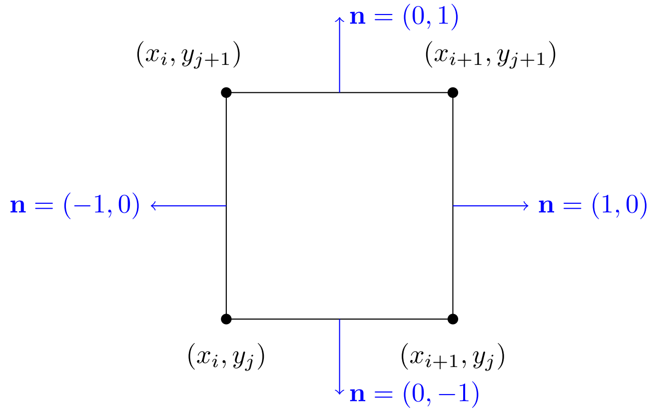

Fig. 2: The boundary ∂R_{xy} and the outward pointing unit normal vector $\mathbf{n} = (n_x, n_y)$ on each side of the boundary.

The forward projection step in equation (3.8) consists of projecting the solution at time t^n onto the staggered grid. It is performed using linear interpolations in two space dimensions in addition to Taylor expansions in space; we obtain:

$$\Delta\mathbf{U}^n_{i+\frac{1}{2},j+\frac{1}{2}} = \frac{1}{2}(\overline{\Delta\mathbf{U}}^n_{i+\frac{1}{2},j} + \overline{\Delta\mathbf{U}}^n_{i+\frac{1}{2},j+1}) - \frac{1}{16}([[\Delta\mathbf{U}^{n,x}]]_{i+\frac{1}{2},j} + [[\Delta\mathbf{U}^{n,x}]]_{i+\frac{1}{2},j+1}) - \frac{1}{16}([[\Delta\mathbf{U}^{n,y}]]_{i,j+\frac{1}{2}} + [[\Delta\mathbf{U}^{n,y}]]_{i+1,j+\frac{1}{2}}). \tag{3.10}$$

Here, $\Delta\mathbf{U}^{n,x}$ and $\Delta\mathbf{U}^{n,y}$ are the spatial partial derivatives of $\Delta\mathbf{U}^n$ that are approximated using the (MC-θ) limiter (3.5).
Finally, the evolution step (3.8) at time t^{n+1} on the staggered nodes can be written as,

$$\begin{aligned}\Delta\mathbf{U}^{n+1}_{i+\frac{1}{2},j+\frac{1}{2}} &= \Delta\mathbf{U}^n_{i+\frac{1}{2},j+\frac{1}{2}} \\ &- \frac{\Delta t}{2}[D^x_+ F(\Delta\mathbf{U}^{n+\frac{1}{2}}_{i,j} + \tilde{\mathbf{U}}_{i,j}) - D^x_+ F(\tilde{\mathbf{U}}_{i,j}) + D^x_+ F(\Delta\mathbf{U}^{n+\frac{1}{2}}_{i,j+1} + \tilde{\mathbf{U}}_{i,j+1}) \\ &\qquad - D^x_+ F(\tilde{\mathbf{U}}_{i,j+1})] \\ &- \frac{\Delta t}{2}[D^y_+ G(\Delta\mathbf{U}^{n+\frac{1}{2}}_{i,j} + \tilde{\mathbf{U}}_{i,j}) - D^y_+ G(\tilde{\mathbf{U}}_{i,j}) + D^y_+ F(\Delta\mathbf{U}^{n+\frac{1}{2}}_{i+1,j} + \tilde{\mathbf{U}}_{i+1,j}) \\ &\qquad - D^y_+ G(\tilde{\mathbf{U}}_{i+1,j})] \\ &\qquad + \Delta t.S(\Delta\mathbf{U}^{n+\frac{1}{2}}_{i,j}, \Delta\mathbf{U}^{n+\frac{1}{2}}_{i+1,j}, \Delta\mathbf{U}^{n+\frac{1}{2}}_{i,j+1}, \Delta\mathbf{U}^{n+\frac{1}{2}}_{i+1,j+1}).\end{aligned} \tag{3.11}$$

Here D^x_+ and D^y_+ are the forward differences given by,
$D^x_+ F(\mathbf{U}_{i,j}) = \frac{F(\mathbf{U}_{i+1,j}) - F(\mathbf{U}_{i,j})}{\Delta x}$, $D^y_+ F(\mathbf{U}_{i,j}) = \frac{F(\mathbf{U}_{i,j+1}) - F(\mathbf{U}_{i,j})}{\Delta y}$.
The predicted values in equation (3.11) are generated at time $t^{n+\frac{1}{2}}$ using a first order

Taylor expansion in time in addition to the balance law (2.1):

$$\Delta\mathbf{U}^{n+\frac{1}{2}}_{i,j} = \Delta\mathbf{U}^{n}_{i,j} + \frac{\Delta t}{2}\left[-\frac{(F^n_{i,j})'}{\Delta x} + \frac{\tilde{F}'_{i,j}}{\Delta x} - \frac{(G^n_{i,j})'}{\Delta y} + \frac{\tilde{G}'_{i,j}}{\Delta y} + S^n_{i,j}\right], \tag{3.12}$$

where $\frac{(F^n_{i,j})'}{\Delta x}$, $\frac{\tilde{F}'_{i,j}}{\Delta x}$, $\frac{(G^n_{i,j})'}{\Delta y}$ and $\frac{\tilde{G}'_{i,j}}{\Delta y}$ denote the approximate flux derivatives with $(F^n_{i,j})' = J_{F^n_{i,j}} \cdot \mathbf{U}^{n,x}_{i,j}$, $\tilde{F}'_{i,j} = J_{\tilde{F}_{i,j}} \cdot \tilde{\mathbf{U}}^{x}_{i,j}$, $(G^n_{i,j})' = J_{G^n_{i,j}} \cdot \mathbf{U}^{n,y}_{i,j}$, $\tilde{G}'_{i,j} = J_{\tilde{G}_{i,j}} \cdot \tilde{\mathbf{U}}^{y}_{i,j}$. Here, we also use the (MC-θ) limiter (3.5) to compute the slopes $\mathbf{U}^{n,x}_{i,j}$, $\tilde{\mathbf{U}}^{x}_{i,j}$, $\mathbf{U}^{n,y}_{i,j}$, and $\tilde{\mathbf{U}}^{y}_{i,j}$ in order to avoid spurious oscillations. $S^n_{i,j}$ is the discrete source term.

In order to retrieve the solution at the time t^{n+1} on the original cells $C_{i,j}$, we project the solution obtained on the ghost cells ($\Delta\mathbf{U}^{n+1}_{i+\frac{1}{2},j+\frac{1}{2}}$) back onto the oroginal grid via linear interpolations in two space dimensions and Taylor expnsions in space,

$$\begin{aligned}\Delta\mathbf{U}^{n+1}_{i,j} = \frac{1}{2}(\overline{\Delta\mathbf{U}}^{n+1}_{i,j-\frac{1}{2}} + \overline{\Delta\mathbf{U}}^{n+1}_{i,j+\frac{1}{2}}) \\ - \frac{1}{16}([[\Delta\mathbf{U}^{n+1,x}]]_{(i),j-\frac{1}{2}} + [[\Delta\mathbf{U}^{n+1,x}]]_{(i),j+\frac{1}{2}}) \\ - \frac{1}{16}([[\Delta\mathbf{U}^{n+1,y}]]_{i-\frac{1}{2},(j)} + [[\Delta\mathbf{U}^{n+1,y}]]_{i+\frac{1}{2},(j)}),\end{aligned} \tag{3.13}$$

where $\Delta\mathbf{U}^{n+1,x}_{i,j}$ and $\Delta\mathbf{U}^{n+1,y}_{i,j}$ denote the spatial partial derivatives of the numerical solution obtained at time t^{n+1} and at the node (x_i, y_j) approximated using the (MC-θ) limiter (3.5).

To complete the presentation of the numerical scheme, we need to verify the well-balanced property of the proposed scheme and to show that it is capable of maintaining stationary solutions of the Euler system with gravitational source term.

Suppose that the numerical solution obtained at time $t = t^n$ satisfies $\mathbf{U}^n_{i,j} = \tilde{\mathbf{U}}_{i,j}$, i.e., $\Delta\mathbf{U}^n_{i,j} = 0$. Performing one iteration using the proposed numerical scheme, one can show that:

1. $\Delta\mathbf{U}^{n+\frac{1}{2}}_{i,j} = 0$.
2. $\Delta\mathbf{U}^{n+1}_{i+\frac{1}{2},j+\frac{1}{2}} = 0$.
3. $\Delta\mathbf{U}^{n+1}_{i,j} = 0$.

In fact, it is straight forward to establish 2 and 3 once 1 is established. We will present the proof of 1 only.

The prediction step (3.12) leads to

$$\begin{aligned}\Delta\mathbf{U}^{n+\frac{1}{2}}_{i,j} = \Delta\mathbf{U}^{n}_{i,j} + \frac{\Delta t}{2}\Bigg[- \frac{F'(\Delta\mathbf{U}^n_{i,j} + \tilde{\mathbf{U}}_{i,j})}{\Delta x} + \frac{F'(\tilde{\mathbf{U}}_{i,j})}{\Delta x} \\ - \frac{G'(\Delta\mathbf{U}^n_{i,j} + \tilde{\mathbf{U}}_{i,j})}{\Delta y} + \frac{G'(\tilde{\mathbf{U}}_{i,j})}{\Delta y} + S(\Delta\mathbf{U}^n_{i,j}, x, y)\Bigg].\end{aligned} \tag{3.14}$$

But since $\Delta\mathbf{U}^n_{i,j} = 0$, then we obtain,

$$\Delta\mathbf{U}^{n+\frac{1}{2}}_{i,j} = \frac{\Delta t}{2}\left[-\frac{F'(\tilde{\mathbf{U}}_{i,j})}{\Delta x} + \frac{F'(\tilde{\mathbf{U}}_{i,j})}{\Delta x} - \frac{G'(\tilde{\mathbf{U}_{i,j}})}{\Delta y} + \frac{G'(\tilde{\mathbf{U}}_{i,j})}{\Delta y}\right].$$

Hence, $\Delta\mathbf{U}^{n+\frac{1}{2}}_{i,j} = 0$. Therefore, we conclude that the updated numerical solution remains stationary up to machine precision.

4. The constrained transport method (CTM). In this work we consider the version of CTM developed in [19]. At the end of each iteration, we apply the CTM corrections to the magnetic field components. Starting from a magnetic field that satisfies the divergence-free constraint $\nabla \cdot \mathbf{B}^n_{i,j} = 0$, we would like to prove $\nabla \cdot \mathbf{B}^{n+1}_{i,j} = 0$. The discrete divergence using central differences at time t^n is given by,

$$\begin{aligned}\nabla \cdot \mathbf{B}^n_{i,j} &= \left(\frac{\partial B_x}{\partial x}\right)^n_{i,j} + \left(\frac{\partial B_y}{\partial y}\right)^n_{i,j}\\ &= \frac{(B_x)^n_{i+1,j} - (B_x)^n_{i-1,j}}{2\Delta x} + \frac{(B_y)^n_{i,j+1} - (B_y)^n_{i,j-1}}{2\Delta y}\\ &= 0.\end{aligned}$$

The vector of conserved variables $\mathbf{U}^{n+1}$ is computed by the numerical scheme, but $\nabla \cdot \mathbf{B}^{n+1}_{i,j}$ might not be zero. Therefore, whenever needed, we correct the components of the magnetic field $\mathbf{B}^{n+1}_{i,j}$ by discretizing the induction equation at the cell centers of $C_{i,j}$,

$$\frac{\partial}{\partial t}\begin{pmatrix} B_x \\ B_y \end{pmatrix} - \frac{\partial}{\partial x}\begin{pmatrix} 0 \\ \Omega \end{pmatrix} + \frac{\partial}{\partial y}\begin{pmatrix} \Omega \\ 0 \end{pmatrix} = 0,$$

where $\Omega = (-\mathbf{u} \times \mathbf{B})_z = -u_x B_y + u_y B_x$. Hence, the discretization of the induction equation is the following,

$$\begin{cases} \dfrac{(B_x)^{n+1}_{i+\frac12,j+\frac12} - (B_x)^n_{i+\frac12,j+\frac12}}{\Delta t} + \dfrac{\Omega^{n+\frac12}_{i+\frac12,j+\frac32} - \Omega^{n+\frac12}_{i+\frac12,j-\frac12}}{2\Delta y} = 0,\\ \dfrac{(B_y)^{n+1}_{i+\frac12,j+\frac12} - (B_y)^n_{i+\frac12,j+\frac12}}{\Delta t} - \dfrac{\Omega^{n+\frac12}_{i+\frac32,j+\frac12} - \Omega^{n+\frac12}_{i-\frac12,j+\frac12}}{2\Delta x} = 0.\end{cases}$$

Then,

$$\begin{cases} (B_x)^{n+1}_{i+\frac12,j+\frac12} = (B_x)^n_{i+\frac12,j+\frac12} - \frac{\Delta t}{2\Delta y}\left(\Omega^{n+\frac12}_{i+\frac12,j+\frac32} - \Omega^{n+\frac12}_{i+\frac12,j-\frac12}\right),\\ (B_y)^{n+1}_{i+\frac12,j+\frac12} = (B_y)^n_{i+\frac12,j+\frac12} + \frac{\Delta t}{2\Delta x}\left(\Omega^{n+\frac12}_{i+\frac32,j+\frac12} - \Omega^{n+\frac12}_{i-\frac12,j+\frac12}\right).\end{cases} \tag{4.1}$$

Now, we compute $\Omega^{n+\frac12}_{i+\frac12,j+\frac12}$ using the numerical solution computed at time t^n and t^{n+1} in order to obtain second order of accuracy in time,

$$\begin{aligned}\Omega^{n+\frac12}_{i+\frac12,j+\frac12} &= \frac12\left[\Omega^{n+1}_{i+\frac12,j+\frac12} + \Omega^n_{i+\frac12,j+\frac12}\right],\\ &= \frac12\left[\Omega^{n+1}_{i+\frac12,j+\frac12} + \frac{\Omega^n_{i,j} + \Omega^n_{i+1,j} + \Omega^n_{i,j+1} + \Omega^n_{i+1,j+1}}{4}\right].\end{aligned}$$

Next, we calculate $\nabla \cdot (\mathbf{B})^{n+1}_{i+\frac12,j+\frac12}$

$$\nabla\cdot(\mathbf{B})^{n+1}_{i+\frac12,j+\frac12} = \frac{(B_x)^{n+1}_{i+\frac32,j+\frac12} - (B_x)^{n+1}_{i-\frac12,j+\frac12}}{2\Delta x} + \frac{(B_y)^{n+1}_{i+\frac12,j+\frac32} - (B_y)^{n+1}_{i+\frac12,j-\frac12}}{2\Delta y}. \tag{4.2}$$

Substituting the magnetic field components on the staggered grid in (4.2) from their values in (4.1) leads to,

$$\nabla \cdot (\mathbf{B})^{n+1}_{i+\frac12,j+\frac12} = \frac14\left[\nabla \cdot \mathbf{B}^n_{i,j} + \nabla \cdot \mathbf{B}^n_{i+1,j+1} + \nabla \cdot \mathbf{B}^n_{i+1,j} + \nabla \cdot \mathbf{B}^n_{i,j+1}\right] = 0. \tag{4.3}$$

Finally, we compute the magnetic field on the main grid $\mathbf{B}_{i,j}^{n+1}$ as the average of its values on the staggered grid,

$$\mathbf{B}_{i,j}^{n+1} = \frac{1}{4}\left[\mathbf{B}_{i+\frac{1}{2},j+\frac{1}{2}}^{n+1} + \mathbf{B}_{i+\frac{1}{2},j-\frac{1}{2}}^{n+1} + \mathbf{B}_{i-\frac{1}{2},j+\frac{1}{2}}^{n+1} + \mathbf{B}_{i-\frac{1}{2},j-\frac{1}{2}}^{n+1}\right].$$

Hence,

$$\nabla \cdot \mathbf{B}_{i,j}^{n+1} = 0. \tag{4.4}$$

5. Numerical Experiments.

A list of numerical experiments has been considered in order to verify the robustness and accuracy of our method. The time-step is computed with CFL number 0.485. The MC-θ limiter is used with $\theta = 1.5$.

5.1. 2D shock tube problem.

For the first numerical test case, we consider a shock tube problem for the system of ideal MHD equations extracted from [1]. The simulation takes place over the computational domain $[-1,1] \times [0,1]$. $U = [\rho, u_1, u_2, u_3, B_2, B_3, p]$ is initially given as $U = [1, 0, 0, 0, \sqrt{4}, 0, 1]$ for $x < 0.5$ and $U = [0.125, 0, 0, 0, -\sqrt{4}, 0, 0.1]$ for $x > 0.5$ and $B_1 = 0.75\sqrt{4}$. This test case features seven discontinuities. It was originally introduced for the non-scaled MHD equations [1]. Hence, dropping π from the initial data makes it a valid test case for the scaled MHD equations. We compute the solution at the final time $t = 0.25$ on 400×400 grid. Because the numerical divergence at the final time was zero, there was no need to apply the CTM. The cross sections in figure 3 show a very good agreement with the results in the literature. In order to investigate the effect of the CTM on the computed solution, we did a convergence study in figure (4) while applying the CTM. As it is very clear in the figures above, applying the CTM for the UC schemes has a small smearing out effect on the solution. For the sake of comparison, we plot a cross section of the energy component with and without applying CTM on a 400×400 grid points in figure 5.

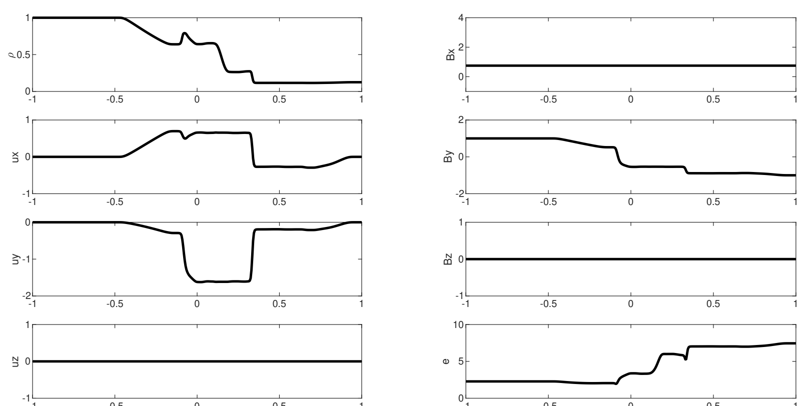

Fig. 3: 2D shock tube problem: cross sections of the 8 components at time $t = 0.25$.

5.2. Four stages Ideal MHD Riemann problem.

This test case is considered to prove the ability of our scheme to solve ideal MHD problems and preserve

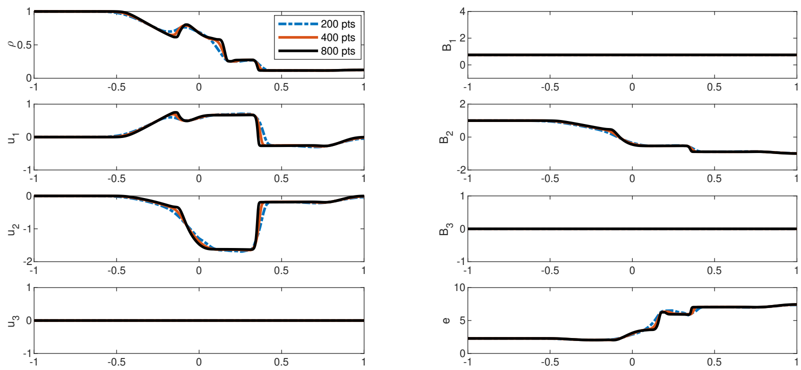

Fig. 4: 2D shock tube problem: cross sections of the 8 components at time $t = 0.25$ on 200×200 (dashed line), 400 × 400 (solid red line), and 800 × 800 (solid black line) grid points.

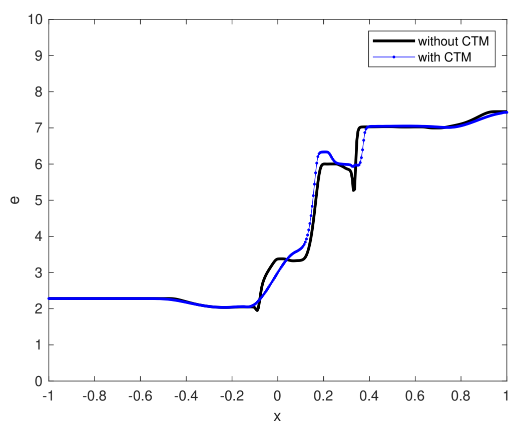

Fig. 5: 2D shock tube problem: a cross section of the energy component at time $t = 0.25$ on 400×400 grid points with and without applying CTM.

the divergence-free constraint. The initial data consist of four constant states [1, 19] . The initial four constant states are given as follows,

$$(5.1) \qquad (\rho, u_1, u_2, p) = \begin{cases} (1, 0.75, 0.5, 1) & \text{if } x > 0 \text{ and } y > 0 \\ (2, 0.75, 0.5, 1) & \text{if } x < 0 \text{ and } y > 0 \\ (1, -0.75, 0.5, 1) & \text{if } x < 0 \text{ and } y < 0 \\ (3, -0.75, -0.5, 1) & \text{if } x > 0 \text{ and } y < 0 \end{cases}$$

with an initial uniform magnetic field $\mathbf{B} = (2, 0, 1)$. The numerical solution is computed in the square $[-1, 1] \times [-1, 1]$ on 400×400 grid points.

Figure 6 illustrates the density at the final time $t_f = 0.8$ with and without applying constrained transport treatment to the magnetic field components. Similar

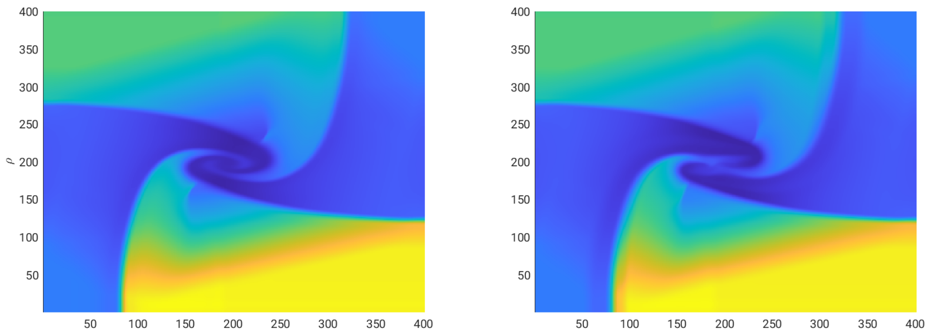

Fig. 6: Four stages Riemann problem: ρ with CTM (left) and without CTM (right) at the final time $t = 0.8$.

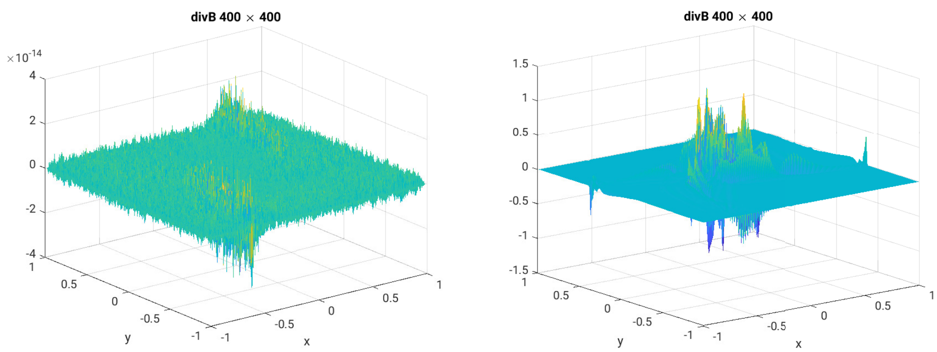

Fig. 7: Four stages Riemann Problem: div$\mathbf{B}$ with CTM (left) and without CTM (right) at the final time $t = 0.8$.

comparison on the divergence of the magnetic field is illustrated in figure 7. The results highlight the robustness of the numerical scheme in the sense that even without treatment we are able to show numerical simulation while other schemes simply blow up without special treatment of the magnetic field.

5.3. MHD vortex. For our third test case, we consider the MHD vortex for the homogeneous ideal MHD equations [2]. The initial data represent a moving stationary solution of the system of the ideal MHD equations and are given by, $r^2 = x^2+y^2$, $\rho = 1$, $u_1 = u_0 - \kappa_p \exp(\frac{1-r^2}{2})y$, $u_2 = v_0 + \kappa_p \exp(\frac{1-r^2}{2})x$, $u_3 = 0$, $B_1 = -m_p \exp(\frac{1-r^2}{2})y$, $B_2 = -m_p \exp(\frac{1-r^2}{2})x$, $B_3 = 0$, and $p = 1 + \left(\frac{m_p^2}{2}(1-r^2) - \frac{\kappa_p^2}{2}\right)$. We set the parameters $m_p = 1, \kappa_p = 1, u_0 = 0$, and $v_0 = 0$. The vortex is advected through the domain $[-5, 5] \times [-5, 5]$ with a velocity (u_0, v_0). Steady state boundary conditions are used in this test case. In figure 8, we present the pressure profile at the final time $t = 100\frac{2\pi}{\sqrt{e}\kappa_p} \approx 100\frac{3.14}{\kappa_p}$ on different grids. The steady state gets preserved exactly as the background solution $\tilde{\mathbf{U}}$ is the vortex itself.

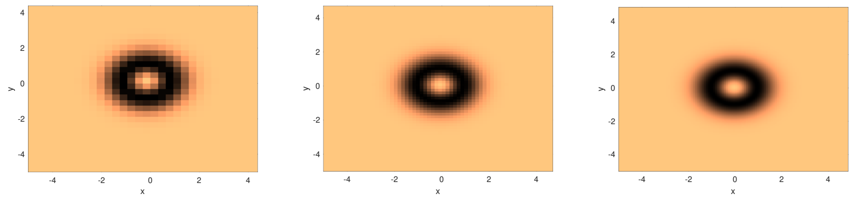

32×32 64×64 128×128

Fig. 8: MHD vortex: pressure profile at the final time on different grid points.

5.4. Hydrodynamic wave propagation. The aim of this test case is to test the well-balanced property of the subtraction method by simulating a steady state solution under hydrodynamic wave propagation. The experiment is carried out in two steps. The first step is to check that the subtraction method preserves the steady state. The initial data are the hydrodynamic steady state in the computational domain $[0,4] \times [0,1]$.

$$\rho(x,y) = \rho_0 \exp(-\frac{y}{H}), p(x,y) = p_0 \exp(-\frac{y}{H}), \mathbf{u} = 0, \mathbf{B} = 0. \tag{5.2}$$

With $H = \frac{p_0}{g\rho_0} = 0.158$, $p_0 = 1.13$ and $g = 2.74$. The subtraction method preserves the hydrodynamic steady state exactly after choosing the reference solution $\tilde{\mathbf{U}}$ at the steady state itself. Figure 9 shows a very simple comparison of the density and the energy cross sections at $t = 0$ and the final time $t = 1.8$. The second step is to add perturbation to the steady state as a time dependent sinusoidal wave that propagates from the bottom boundary of the vertical velocity and exits from the top one. The wave formula is the following,

$$u^n_{2_{i,\{0,-1\}}} = \exp(-100(x_{i,\{0,-1\}} - 1.9)^2) c \sin(6\pi t^n). \tag{5.3}$$

The bottom boundary is a localized piston at $x = 1.9$. Figure 10 shows the profile of the wave at the final time $t = 1.8$ for $c = 0.003$ (left) and for $c = 0.3$ (right) for 800×200 grid points. The waves propagate in both cases from bottom to top under the effect of the pressure and gravity forces. The case where $c = 0.003$ models a small perturbation and $c = 0.3$ models a stronger wave. The results are in a very good agreement with the ones in [7]. Additionally, they match the results of the most accurate (third order) of the three schemes compared in [7]. Hence, the scheme is well-balanced in the sense that it preserves the steady state and can capture its perturbations.

5.5. MHD wave propagation. In this test case, we model propagating waves that not only undergo the effects of pressure and gravity, but also that of the magnetic field. The test case is extracted from [7]. We consider the magnetohydrodynamic steady state defined as,

$$\rho(x,y) = \rho_0 \exp(-\frac{y}{H}), p(x,y) = p_0 \exp(-\frac{y}{H}), \mathbf{u} = 0, \mathbf{B} = (0,\mu,0), \nabla \cdot \mathbf{B} = 0. \tag{5.4}$$

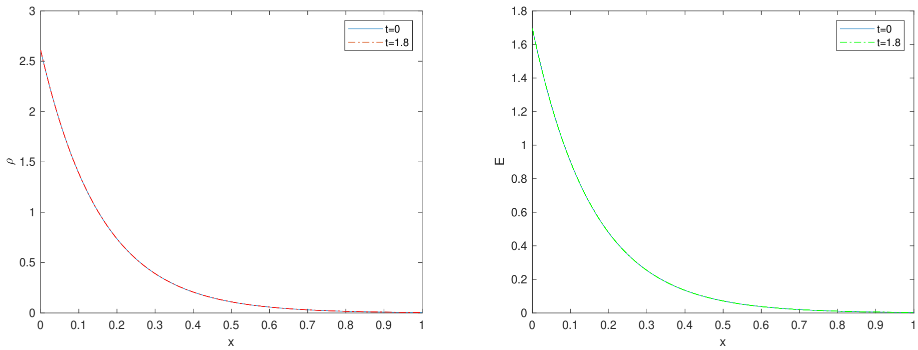

Fig. 9: Hydrodynamic wave propagation: a comparison of the cross sections of the density ρ (left) and the energy E (right) initially and at the final time $t = 1.8$.

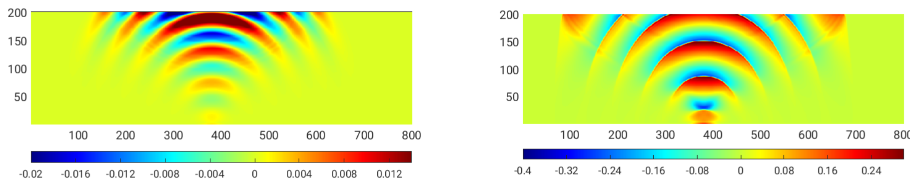

Fig. 10: Hydrodynamic wave propagation: wave profile u_2 for $c = 0.003$ (left) and $c = 0.3$ (right) at the final time $t = 1.8$.

Where μ is a parameter that takes different values for each part of the experiment. The waves model a perturbation of the steady state that starts from the bottom boundary of the normal velocity as follows,

$$\mathbf{u}^n_{i,\{0,1\}} = \begin{cases} \frac{\mathbf{B}_{i,\{0,1\}}}{|\mathbf{B}_{i,\{0,1\}}|} c \sin(6\pi t^n) & \text{for } x \in [0.95, 1.05], \\ 0 \quad \text{Otherwise}, \end{cases} \tag{5.5}$$

with $c = 0.3$. The computational domain is $[0, 2] \times [0, 1]$. We use the wave propagation boundary conditions suggested in [7]. These boundary conditions are periodic boundaries in the x-direction for $\mathbf{U}$ and p and Neumann type boundary conditions in the y-direction as the following,

$$\rho^n_{i,1} = \rho^n_{i,2} e^{\frac{\Delta y}{H}}, \rho^n_{i,0} = \rho^n_{i,1} e^{\frac{\Delta y}{H}}$$

$$\rho^n_{i,ny-1} = \rho^n_{i,ny-2} e^{\frac{-\Delta y}{H}}, \rho^n_{i,ny} = \rho^n_{i,ny-1} e^{\frac{-\Delta y}{H}}$$

for $1 \le i \le nx$. Similar boundary conditions for the momentum $\rho\mathbf{u}$ and the pressure p. Energy boundary conditions are computed from the pressure. For the magnetic field boundary conditions, we simply copy the data from the cell before. We present the profile of the velocity in the direction of the magnetic field,

$$u_B = <\mathbf{u}, \mathbf{B}> / |\mathbf{B}|, \tag{5.6}$$

at the final time $t = 0.54$ for different values of μ. As μ increases, the effect of the magnetic field on the propagating wave increases. The wave profile gets compressed as the magnetic field takes higher values. The plasma parameter is given by $\beta = \frac{2p}{\mathbf{B}^2}$ [7]. It measures the relative strength of the thermal pressure to the magnetic field, and is crucial in determining the dynamics of the plasma. The β-isolines are illustrated in black and the lines of the magnetic field are illustrated in white. The parameter β indicates the effects of the pressure and the magnetic field on the propagating wave such that, for $\beta > 1$, the region is pressure dominated, while for $\beta < 1$, the region is magnetic field dominated. In figure 11, the profile of the velocity in the direction of the magnetic field, in the case of μ almost zero, is illustrated, which is exactly the velocity in the y-direction in this case. The wave propagates freely along the computational domain taking a radial profile in the absence of the magnetic field on 400×200 grid points. Figure 12, shows the profile of the propagating wave under the effect of a stronger magnetic field for $\mu = 1$ on 400×200 grid points without applying CTM. In addition, figure 12 presents the divergence of the magnetic field which is clearly not zero. On the other hand, we present the same results with applying CTM on 1200×600 grid points in figure 13. Applying the CTM results in a zero discrete divergence of the magnetic field up to machine precision. Another effect of applying the CTM is the diffusion we see in figure 13, which was resolved by evolving the solution on a finer grid. Additionally, we present the velocity in the direction perpendicular to the magnetic field in figure 14 for $\mu = 1$ at different times.
Our results, obtained with the second order scheme, are comparable with the results in [7], obtained with third order schemes, which ensures the robustness of our scheme and its capability of solving physically challenging problems, such as wave propagation under the effect of pressure and gravity.

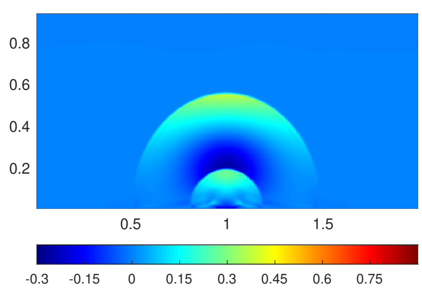

Fig. 11: MHD wave propagation: velocity in a direction parallel to the magnetic field $u_B =< \mathbf{u}, \mathbf{B} > /|\mathbf{B}|$ for $\mu = 0$ on 400×200 grid points at the final time $t = 0.54$.

6. Conclusion. In conclusion, we develop a two-dimensional second order unstaggered finite volume central scheme for the system of MHD equations. The proposed scheme is capable of preserving any type of known equilibrium states due to a special reformulation that computes the numerical solution in terms of a specific reference state. A comparison between the obtained numerical results and the corresponding literature ensures the robustness and the accuracy of the developed schemes. In this work, we chose the CTM as a procedure to clean the divergence of the magnetic field, which is applied dynamically whenever needed. Meaning that, in the test

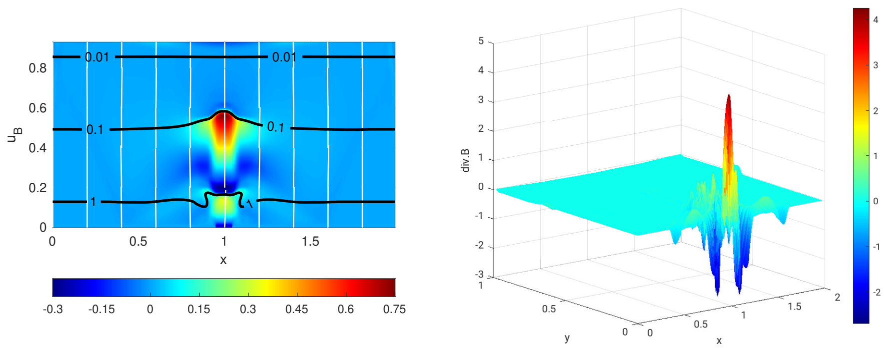

Fig. 12: MHD wave propagation: velocity in a direction parallel to the magnetic field $u_B =< \mathbf{u}, \mathbf{B} > /|\mathbf{B}|$ for $\mu = 1$ on 400×200 grid points at the final time $t = 0.54$ without CTM.

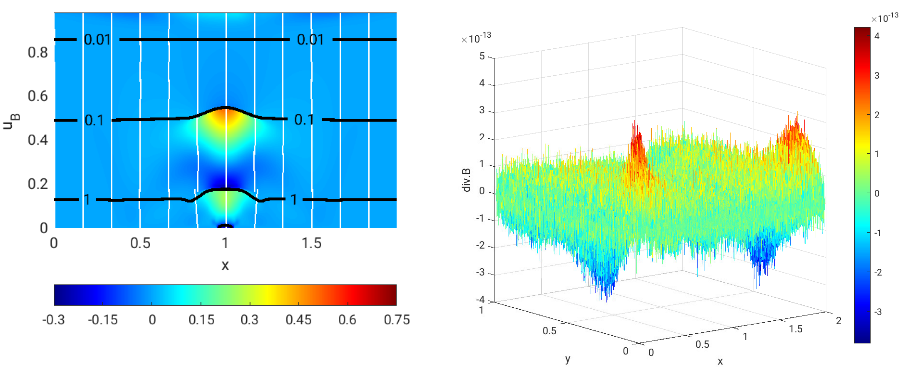

Fig. 13: MHD wave propagation: velocity in a direction parallel to the magnetic field $u_B =< \mathbf{u}, \mathbf{B} > /|\mathbf{B}|$ for $\mu = 1$ on 1200×600 grid points at the final time $t = 0.54$ with CTM.

cases where the numerical divergence is zero at the final time and no numerical instabilities had been observed, we do not apply it. This leaves us with a second order well-balanced finite volume numerical scheme that captures solutions of the MHD equations and satisfies the divergence-free constraint. All our computations are done on a Cartesian grid in 2D. A triangular mesh can be considered in future work.

7. Funding. The authors would like to acknowledge the National Council for Scientific Research of Lebanon (CNRS-L) for granting a doctoral fellowship to Farah Kanbar.

REFERENCES

[1] P. Arminjon and R. Touma, *Central finite volume methods with constrained transport divergence treatment for ideal MHD*, Journal of Computational Physics, 204 (2005), pp. 737–

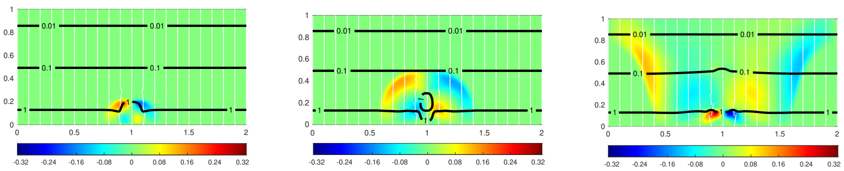

$u_{\perp B}$ at t = 0.216 $u_{\perp B}$ at t = 0.36 $u_{\perp B}$ at t = 0.504

Fig. 14: MHD wave propagation: velocity perpendicular to the magnetic field $u_{\perp B} =< (u_1, u_2), (-B_2, B_1) > /|\mathbf{B}|$ for $\mu = 1$ on 400×200 grid points at different times.

759.

[2] J. Berberich, P. Chandrashekar, and C. Klingenberg, *High order well-balanced finite volume methods for multi-dimensional systems of hyperbolic balance laws*, journal of computational physics, (2019).

[3] T. J. Bogdan and et al, *Waves in the magnetized solar atmosphere ii : waves from localized sources in magnetic flux concentrations*, Astrophys.J., 599 (2003), pp. 626–660.

[4] J. U. Brackbill and D. Barnes, *The effect of nonzero divb on the numerical solution of the magnetohydrodynamic equations*, J. Comput. Phys., 35 (1980), pp. 426–430.

[5] J. U. Brackbill and D. C. Barnes, *The effect of nonzero* $\nabla.\boldsymbol{B}$ *on the numerical solution of the magnetohydrodynamic equations*, J. Comp. Phys., 201 (2004), pp. 261–285.

[6] C. R. Evans and J. F. Hawley, *Simulation of magnetohydrodynamic flows: A constrained transport method*, Astrophys. J.Lett., 332 (1988), p. 659.

[7] F. Fuchs, A. McMurry, S. Mishra, N. Risbro, and K. Waagan, *High order well-balanced finite volume schemes for simulating wave propagation in stratified magnetic atmospheres*, Journal of Computational Physics, 229 (2010), pp. 4033–4058.

[8] S. K. Godunov, *The symmetric form of magnetohydrodynamics equation*, Numer. Methods Mech. Contin. Media 1, 26 (1972).

[9] G. S. Jiang, D. Levy, C. T. Lin, S. Osher, and E. Tadmor, *High-resolution nonoscillatory central schemes with nonstaggered grids for hyperbolic conservation laws*, SIAM Journal on Numerical Analysis, 35 (1998), pp. 2147–2168.

[10] F. Kanbar, R. Touma, and C. Klingenberg, *Well-balanced central schemes for the one and two-dimensional euler systems with gravity*, Applied Numerical Mathematics, 156 (2020), pp. 608–626.

[11] H. Nessyahu and E. Tadmor, *Non-oscillatory central differencing for hyperbolic conservation laws*, Journal of Computational Physics, 87 (1990), pp. 408–463.

[12] K. Powell, P. Roe, T. Linde, T. Gombosi, and D. D. zeeuw, *A solution adaptive upwind scheme for ideal mhd*, J. Comput. Phys., 154 (1999), pp. 284–309.

[13] K. G. Powell, *An approximate riemann solver for magnetohydrodynamics (that works in more than one dimension)*, ICASE-Report 94-24 (NASA CR-194902) (NASA Langley Research Center, Hampton, VA 23681-0001, 8. April 1994).

[14] K. G. Powell, *An approximate riemann solver for magnetohydrodynamics (that works in more than one space dimension)*, Technical report, 94-24, ICASE, Langley, VA, (1994).

[15] K. G. Powell, P. L. Roe, R. S. Myong, T. Gombosi, and D. D. Zeeuw, *An upwind scheme for the magnetohydrodynamics*, AIAA Paper 95-1704-CP, (1995).

[16] C. S. Rosenthal and et al, *Waves in the magnetized solar atmosphere i: Basic processes and internetwork oscillations*, Astrophys.J., 564 (2002), pp. 508–524.

[17] G. Toth, *The divb=0 constraint in shock capturing magnetohydrodynamics codes*, J. Comput. Phys., 161 (2000), pp. 605–652.

[18] R. Touma, *Central unstaggered finite volume schemes for hyperbolic systems: Applications to unsteady shallow water equations*, Applied Mathematics and Computation, 213 (2009), pp. 47–59.

[19] R. Touma, *Unstaggered central schemes with constrained transport treatment for ideal and shallow water magnetohydrodynamics*, Applied Numerical Mathematics, 60 (2010), pp. 752–766.

[20] R. Touma, *Unstaggered central schemes with constrained transport treatment for ideal*

and shallow water magnetohydrodynamics, Applied Numerical Mathematics, 60 (2010), pp. 752–766.

[21] R. Touma and S. Khankan, *Well-balanced unstaggered central schemes for one and two-dimensional shallow water equation systems*, Applied Mathematics and Computation, 218 (2012), pp. 5948–5960.

[22] R. Touma and C. Klingenberg, *Well-balanced central finite volume methods for the ripa system*, Applied Numerical Mathematics, 97 (2015), pp. 42–68.

[23] R. Touma, U. Koley, and C. Klingenberg, *Well-balanced unstaggered central schemes for the euler equations with gravitation*, SIAM J. Sci. Comput., 38 (2016), pp. 773–807.